Supporting Information

Laser-induced nano-bismuth decorated CdS-graphene hybrid for plasmon-enhanced photoelectrochemical analysis

Hui Li, Xin Xia, Chengxiang Guo, Lei Ge,* and Feng Li*

College of Chemistry and Pharmaceutical Sciences, Qingdao Agricultural University,
Qingdao, 266109, People's Republic of China

*Corresponding author: Feng Li, Lei Ge

E-mail: lifeng@qau.edu.cn; lge@qau.edu.cn

Telephone: +86-532-58957855

EXPERIMENTAL SECTION

Reagents and materials. Bismuth(Ⅲ) nitrate pentahydrate ($Bi(NO_3)_3\cdot 5H_2O$), cadmium(II) acetylacetonate ($Cd(acac)_2$), sodium sulfide nonahydrate ($Na_2S\cdot 9H_2O$), ascorbic acid (AA), dimethyl sulfoxide (DMSO), and N,N-dimethylformamide (DMF) were purchased from Sigma-Aldrich Chemical Co. (St. Louis, MO, USA). Polyethersulfone (PES) polymer pellets were obtained from Trump Chemical Corporation. ITO slices (1.0 × 4.0 cm) were purchased from China Southern Glass Holding Co., Ltd (ITO coating thickness of 180±20 nm with a sheet resistance of 8.1 ± 0.6 Ω/square). The ITO slices were ultrasonically cleaned in acetone, ethanol, and water, respectively, for 30 min each, followed by washing copiously with ultrapure water and blown dry under a stream of N_2 gas. The ultrapure water (resistivity of 18.2 MΩ cm at 25 °C) was provided by a Milli-Q water purification system (Millipore Corp., Bedford, MA, USA).

Fabrication of LI-Bi^0-CdS-G@ITO photoelectrode. The LI-Bi^0-CdS-G@ITO photoelectrode was prepared by straightforward laser-scribing technology. Briefly, 67.2 mg $Bi(NO_3)_3\cdot 5H_2O$ and 56 mg $Cd(acac)_2$ were successively dissolved in 1 : 4 (v/v) DMSO/DMF mixed solvent (5 mL) under continuous magnetic stirring at room temperature. Subsequently, 0.5 g PES polymer were dissolved into the above mixture with the aids of vigorous stirring overnight to obtain a homogeneous metal ion-containing PES solution (Bi^{3+}/Cd^{2+}−PES). The resulting mixture (60 μL) was then drop-coated onto the surface of freshly cleaned ITO slices with a fixed geometrical area of 1×1 cm^2, followed by vacuum drying at 80 °C for 2 h to evaporate the solvent.

After natural cooling down to room temperature, the Bi^{3+}/Cd^{2+}−PES membrane coated ITO glass (Bi^{3+}/Cd^{2+}−PES@ITO) were scanned by 10.6 μm CO_2 infrared laser in a consumer-grade laser cutting machine (Epilog Laser MINI), where the Bi^{3+}/Cd^{2+}−PES membranes were directly transformed into LI-Bi^0-CdS-G nanohybrid adhered on the ITO glass surface. The DPI (dots per inch), output power, z-distance, and scan rate of this CO_2 infrared laser were fixed at 1200, 6.0 W, 52.0 mm (2.0 mm defocus), and 166 mm s^{-1}, respectively. As a comparison, LIG@ITO, LI-Bi^0-G@ITO, and LI-CdS-G@ITO electrodes were also fabricated analogously under the same conditions without the addition of $Bi(NO_3)_3 \cdot 5H_2O$ and/or $Cd(acac)_2$.

Characterizations. X-ray diffraction (XRD) patterns were collected with a Bruker D8 diffractometer (Germany) using Cu Kα as the radiation source over the 2θ range of 20−70°. X-ray photoelectron spectroscopy (XPS) measurements were performed on a ESCALAB 250Xi instrument (Thermo Fisher, Waltham, MA, Al Kα radiation). Scanning electron microscopy (SEM) images were recorded using a HITACHI S-4800 electron microscopy operating at an accelerating voltage of 2.0 kV. Transmission electron microscopy (TEM) images, high-resolution transmission electron microscopy (HRTEM) images were obtained on a FEI microscope (Tecnai G2 F30) at 300 kV accelerating voltage. Raman spectra were measured by a DXRxi Raman spectrometer (Thermo Scientific) with an excitation wavelength of 532 nm.

Electrochemical and PEC measurements. The PEC measurements were performed on a Zahner PEC measurement system (Zahner-Elektrik GmbH & Co. KG, Germany) at a constant potential of 0.0 V (vs Ag/AgCl) using a ~634 nm light emitting diode (LED, 0.8 W/cm^2) as the light source. Unless other indicated, the supporting electrolyte for PEC measurements was 0.1 M phosphate buffered saline (PBS, pH = 7.4) containing 0.1 M ascorbic acid (AA) as sacrificial electron donor. Electrochemical impedance spectroscopy (EIS) measurements were performed on an Autolab electrochemical workstation (Metrohm, The Netherlands) in the frequency range of 100 kHz to 0.01 Hz using 5 mM $[Fe(CN)_6]^{3-/4-}$ (1:1) mixture as redox probes. Both PEC and EIS measurement was carried out in a conventional three-electrode system with a laser-scribed ITO glass as working electrode, a Pt wire as counter electrode, and an Ag/AgCl as reference electrode. For S^{2-} detection, N_2-saturated 10 mM M KOH aqueous solution containing S^{2-} at different concentration was used as the electrolyte.

For water sample analysis, local river water was employed to prepare the spiked samples in this work. Prior to use, 1.0 mL river water sample was first filtered through a 0.2 μm hydrophilic cellulose acetate filter and then diluted by 20 mM KOH solution to 2.0 mL, followed by centrifugation at 12000 rpm for 3 min and then N_2 bubbling throughout the supernatant for 15 min to remove dissolved O_2. Subsequently, different amounts of Na_2S were spiked into the above river water sample, resulting in final S^{2-} concentrations of 0.5 μM, 5.0 μM, and 50 μM, respectively. The obtained water samples were finally measured under the same conditions mentioned above.

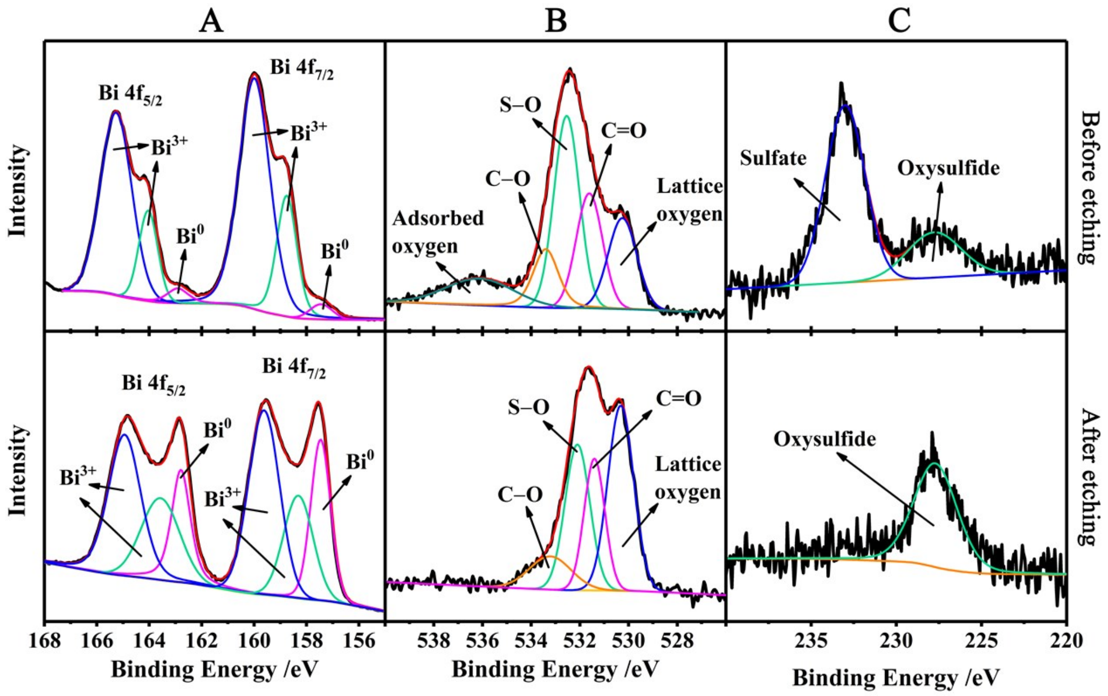

Fig. S1. High resolution (A) Bi 4f, (B) O 1s, and (C) S 2s XPS spectra of LI-Bi^{0}-G@ITO photoelectrode before (top panel) and after (bottom panel) etching.

In the Bi 4f spectrum (Fig. S1A) of LI-Bi^{0}-G@ITO, the characteristic peaks centered at approximately 165.1 and 159.8 eV belong to the binding energies of Bi^{3+}.[1] The Bi 4f$_{7/2}$ and Bi 4f$_{5/2}$ peaks at around 164.1 and 158.8 eV (Fig. S1A) is typically assigned to the characteristic peaks of suboxide species due to the oxygen vacancies.[2] After surface etching, the two Bi 4f peaks of LI-Bi^{0} at around 162.8 and 157.5 eV[3] (Fig. S1A, bottom) were enhanced. Fig. S1B (top) shows that the fine scan of the O 1s spectrum of the LI-Bi^{0}-G@ITO photoelectrode can be resolved into five peaks before etching. The peak at the binding energy of 530.3 eV is typically assigned to lattice oxygen, which is generated from the Bi−O bonds in Bi_2O_3.[4] The peaks located at around 533.4 eV, 532.5 eV, and 531.5 eV are characteristic of C−O, S−O, and C=O groups, respectively.[5] After surface etching, the adsorbed oxygen (536.2 eV) peak[5] vanishes in the O 1s spectrum of the LI-Bi^{0}-G@ITO photoelectrode (Fig. S1B, bottom). Fig. S1C (top) presents the XPS peak of S 2s before etching fitted with two peaks. The S 2s peaks at around 227.7 eV can be assigned to the oxysulfide group.[6] The binding energies at 233.0 eV are attributed to the existence of different oxygen-containing sulfur groups (C−SO$_x$, x = 2, 3, 4, respectively),[6] which disappears after the surface etching (Fig. S1C, bottom).

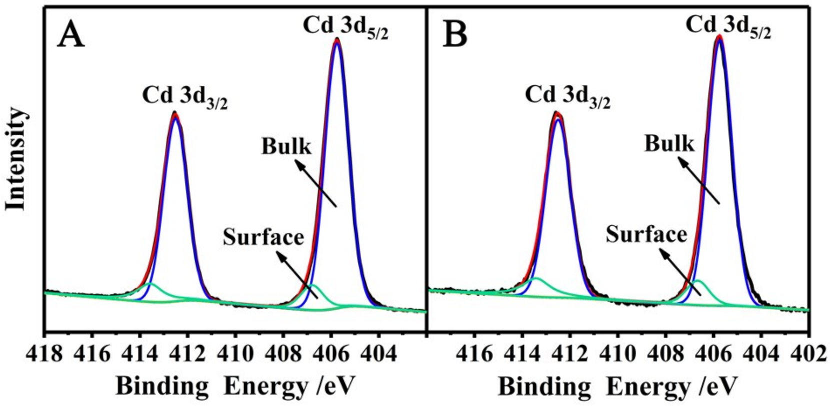

Fig. S2. High resolution Cd 3d XPS spectra of LI-Bi^0-CdS-G@ITO photoelectrode before (A) and after (B) etching.

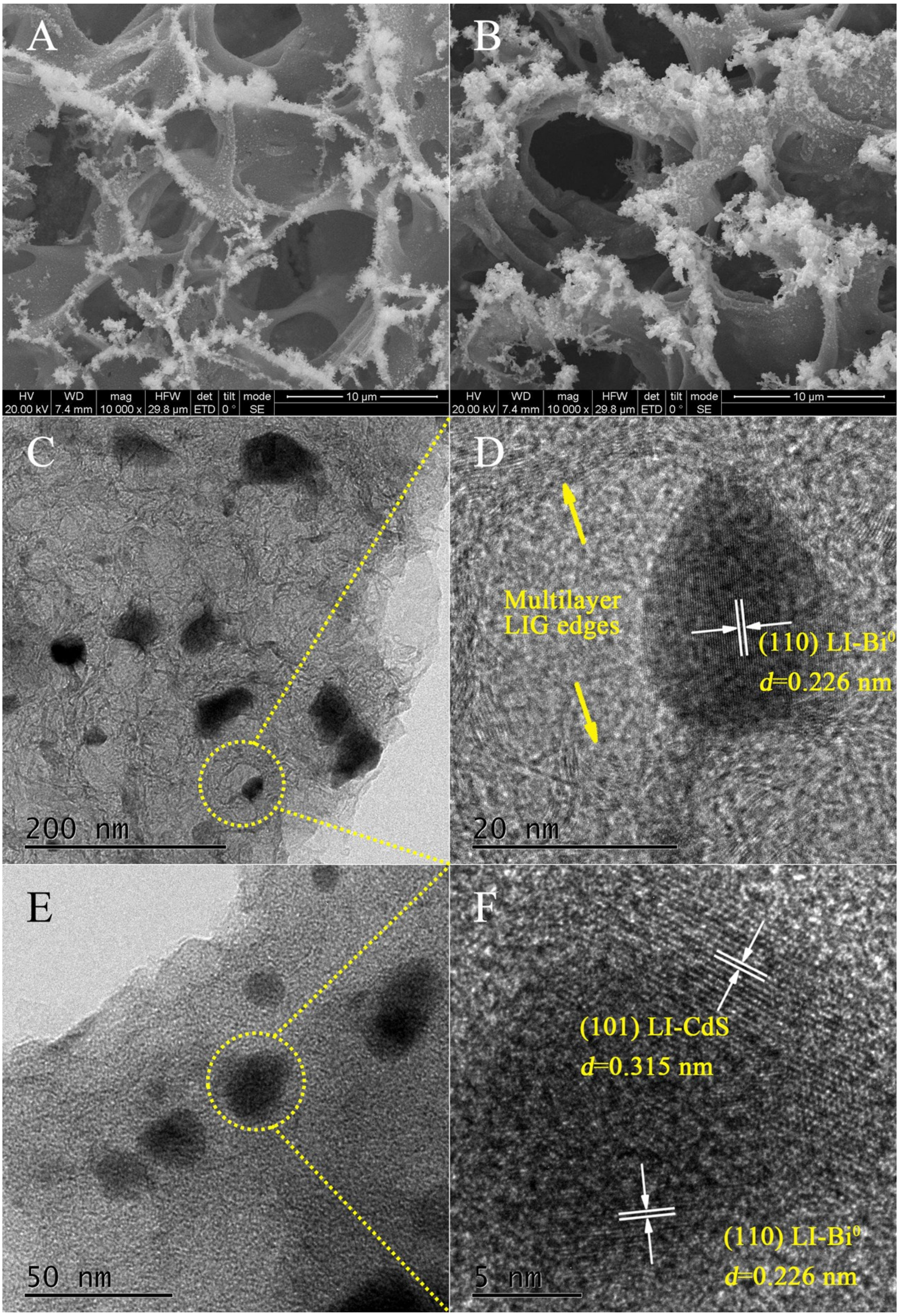

Fig. S3. SEM image of (A) LI-Bi0-G@ITO photoelectrode and (B) LI-Bi^0-CdS-G@ITO photoelectrode. (C and E) TEM and (D and F) HRTEM image of (C and D) LI-Bi^0-G nanocomposite and (E and F) LI-Bi^0-CdS-G nanocomposite.

The SEM image (Fig. S3A) shows that LI-Bi^0-G@ITO consists of interconnected multi-layered LIG sheets with rough surfaces and edges. This typical 3D macroporous network structure with a highly accessible surface area was formed by the laser-induced rapid liberation of gaseous product under extremely high localized temperatures. When $Cd(acac)_2$ as a precursor of LI-CdS was introduced, no obvious change of the 3D interconnected macroporous framework was observed from LI-Bi^0-CdS-G@ITO (Fig. S3B). The 3D macroporous conductive LIG scaffold can not only favor the exposure of more PEC active sites but also accelerate the mass transport within the hybrid photoelectrode, which could further improve the PEC performance. The TEM image of LI-Bi^0-G hybrids in Fig. S3C demonstrates the well dispersion of LI-Bi^0 nanocrystals, with diameters of approximately 20−70 nm, on the multilayered LIG nanosheet. As marked in high-resolution TEM image (Fig. S3D), the clear lattice *d*-spacing of 0.226 nm corresponds to the (110) plane of metal LI-Bi^0 and no lattice fringe could be assigned to Bi_2O_3, which is in accordance with the XRD results. For LI-Bi^0-CdS-G nanohybrids, Fig. S3E,F reveals that the laser-induced Bi^0-CdS nanocomposites are well embedded in the multi-layered LIG with sizes of 20−40 nm and display clear lattice fringes in the high-resolution TEM image. As illustrated in Fig. S3F, the lattice *d*-spacing of 0.315 nm evidently matched the (101) crystal plane of the hexagonal phase of LI-CdS. Besides, the fringe *d*-spacing of 0.226 nm corresponding to the (110) lattice plane of LI-Bi^0 could also be observed.

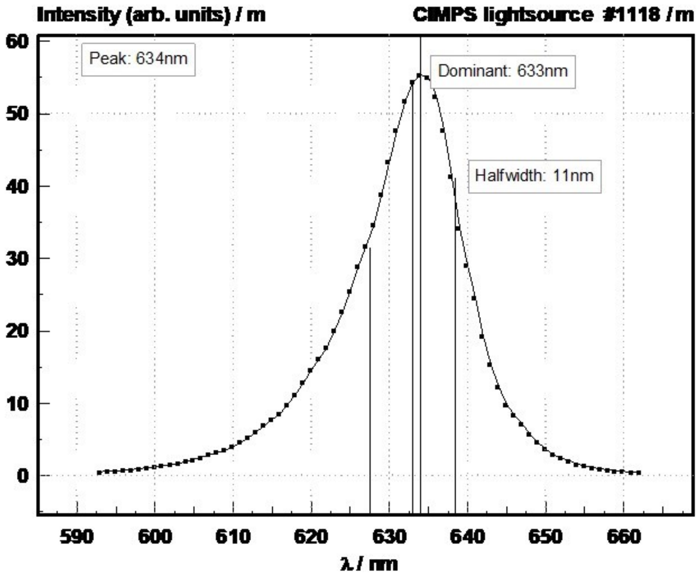

Fig. S4. Calibrated emission spectrum of the red LED light source used in this work from Zahner PEC measurement system.

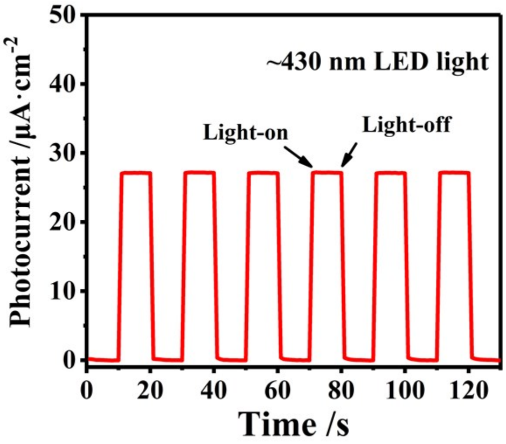

Fig. S5. Photocurrent response of LI-CdS-G@ITO photoelectrode under the irradiation of ~430 nm light.

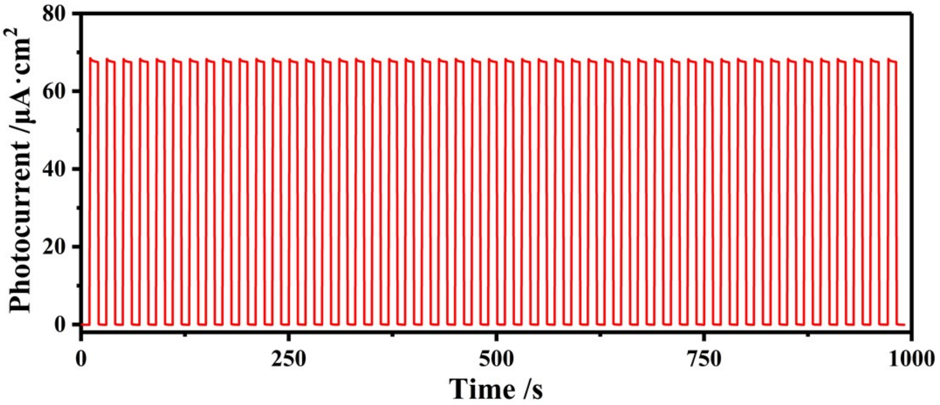

Fig. S6. Stability test of LI-Bi^{0}-CdS-G@ITO photoelectrode under repeated on/off illumination cycles.

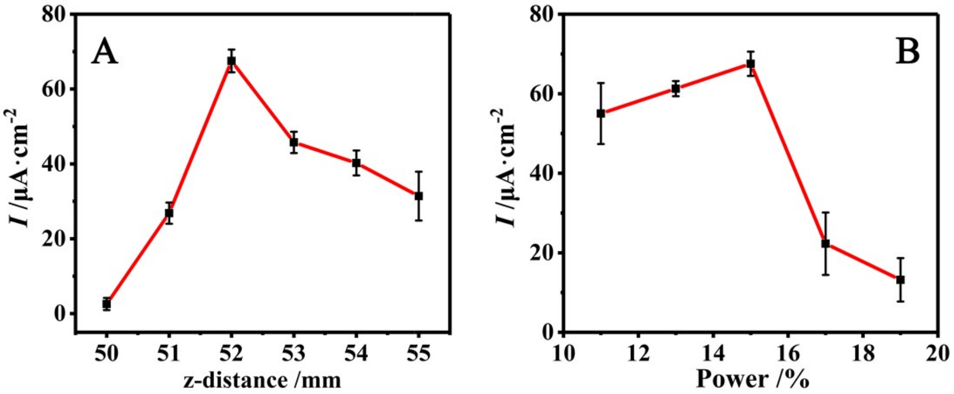

Fig. S7. Impact of laser *z*-distance (A) and laser power (B) on the photocurrent response of LI-Bi^{0}-CdS-G@ITO photoelectrode. The full laser power is 40 W.

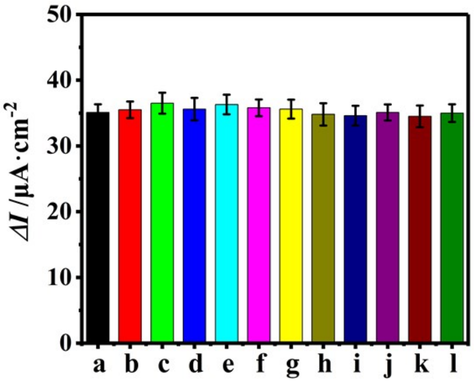

Fig. S8. Photocurrent response of the proposed LI-Bi^0-CdS-G@ITO photoelectrode towards (a) 10.0 μM S^{2-} alone or with the coexistence of (b) Cl^-, (c) I^-, (d) F^-, (e) Br^-, (f) SO_4^{2-}, (g) SO_3^{2-}, (h) CH_3COO^-, (i) CO_3^{2-}, (j) NO_3^-, (k) PO_4^{3-}, and (l) SCN^- at the concentrations of 10.0 μM.

Table S1. Assay performance comparison of our method with other S^{2-} sensors.

Methods	Linear range	Detection limit	Reference
Fluorescence	0 μM to 10 μM	1.35 μM	7
Fluorescence	2.0 μM to 10 μM	0.32 μM	8
Fluorescence	0.2 μM to 30 μM	0.21 μM	9
Fluorescence	1.0 μM to 10 μM	0.48 μM	10
Fluorescence	0.5 μM to 12 μM	0.42 μM	11
Fluorescence	5.0 μM to 110.0 μM	0.286 μM	12
Fluorescence	---	2.1 μM	13
Fluorescence	0.06 mM to 60 mM	0.02 mM	14
Fluorescence	50 μM to 1000 μM	50 μM	15
Colorimetry	0 μM to 10 μM	0.3 μM	16
Colorimetry	0.5 μM to 15 μM	0.28 μM	17
Colorimetry	5 μM to 15 μM	3 μM	18
Colorimetry	12.5 μM to 500 μM	8.1 μM	19
Colorimetry	0.5 μM to 10 μM	80 nM	20

Absorption	0.5 μM to 7.5 μM	0.15 μM	[21]
Electrochemiluminescence	0 μM to 100 μM	20 nM	[22]
Electrochemiluminescence	0.05 μM to 100 μM	27 nM	[23]
Phosphorescence	2.67 μM to 596 μM	0.138 μM	[24]
Optofluidic laser	0.01 μM to 10 μM	0.01 μM	[25]
Electrochemistry	1 μM to 100 μM	0.7 μM	[26]
Photoelectrochemistry	0.1 μM to 100 μM	30 nM	This work

Table S2. Recoveries of the proposed PEC sensor for S^{2-} spiked river water samples

Samples	Spiked (μM)	Measured (μM)	Recovery (%)
sample-1	0.50	0.53 ± 0.05	106
sample-2	5.0	4.8 ± 0.4	96
sample-3	50	51 ± 1	102

References

1 Y. Yu, C. Cao, H. Liu, P. Li, F. Wei, Y. Jiang and W. Song, *J. Mater. Chem. A*, 2014, **2**, 1677.
2 L. Yan, Z. Gu, X. Zheng, C. Zhang, X. Li, L. Zhao and Y. Zhao, *ACS Catal.*, 2017, **7**, 7043.
3 X. Zhang, S. Yu, Y. Liu, Q. Zhang and Y. Zhou, *Appl. Surf. Sci.*, 2017, **396**, 652.
4 H. Xu, X. Hu, H. Yang, Y. Sun, C. Hu and Y. Huang, *Adv. Energy Mater.*, 2015, **5**, 1401882.
5 H. Li, C. Guo, C. Liu, L. Ge and F. Li, *Analyst*, 2020, **145**, 4041.
6 L. Qiu and G. Xu, *Appl. Surf. Sci.*, 2010, **256**, 3413.
7 L. Tang, M. Cai, Z. Huang, K. Zhong, S. Hou, Y. Bian and R. Nandhakumar, *Sens. Actuators, B*, 2013, **185**, 188.
8 A. Barati, M. Shamsipur and H. Abdollahi, *Sens. Actuators, B*, 2016, **230**, 289.
9 Y. Wu, X. Wu, B. Niu, Y. Zeng, M. Zhu and H. Guo, *Sens. Actuators, B*, 2018, **255**, 3163.
10 A. Abi, G. Kazemi and A. Safavi, *Sens. Actuators, B*, 2018, **277**, 1.
11 Y. Wang, J. Hu, Q. Zhuang and Y. Ni, *ACS Sustainable Chem. Eng.*, 2016, **4**, 2535.
12 G. Zhang, R. Wang, L. Shi, C. Zhang, Y. Zhang, Y. Zhou, C. Dong, G. Li and S. Shuang, *Sens. Actuators, B*, 2019, **279**, 361.
13 J. Chen, Y. Li, W. Zhong, Q. Hou, H. Wang, X. Sun and P. Yi, *Sens. Actuators, B*, 2015, **206**, 230.
14 R. Pol, F. Céspedes, D. Gabriel and M. Baeza, *Sens. Actuators, B*, 2019, **290**, 364.
15 N. Xu, H.-W. Li, Y. Yue and Y. Wu, *Nanotechnology*, 2016, **27**, 425602.

16 J. Zhang, X. Xu, Y. Yuan, C. Yang and X. Yang, *ACS Appl. Mater. Interfaces*, 2011, **3**, 2928.
17 C. Chen, D. Zhao, L. Lu, F. Yang and X. Yang, *Sens. Actuators, B*, 2015, **220**, 1247.
18 J. Zhang, X. Xu and X. Yang, *Analyst*, 2012, **137**, 1556.
19 A. Hatamie, B. Zargar and A. Jalali, *Talanta*, 2014, **121**, 234.
20 H.-H. Deng, S.-H. Weng, S.-L. Huang, L.-N. Zhang, A.-L. Liu, X.-H. Lin and W. Chen, *Anal. Chim. Acta*, 2014, **852**, 218.
21 L. Liu, Y. Wang and W. Fu, *Sens. Actuators, B*, 2017, **247**, 414.
22 H. J. Kim, T. Kim and J.-I. Hong, *Sens. Actuators, B*, 2020, **307**, 127656.
23 Z.-X. Wang, C.-L. Zheng, Q.-L. Li and S.-N. Ding, *Analyst*, 2014, **139**, 1751.
24 T. Zhou, N. Wang, C. Li, H. Yuan and D. Xiao, *Anal. Chem.*, 2010, **82**, 1705.
25 C. Gong, Y. Gong, M. K. Khaing Oo, Y. Wu, Y. Rao, X. Tan and X. Fan, *Biosens. Bioelectron.*, 2017, **96**, 351.
26 K. S. Shalini Devi and A. Senthil Kumar, *Analyst*, 2018, **143**, 3114.